

η^6 -Metalated Aryl Iodides in Diels-Alder Cycloaddition Reactions: Mode of Activation and Catalysis

 Susana Portela and Israel Fernández^{*[a]}

Abstract: The potential application of η^6 -metalated aryl iodides as organocatalyst has been explored by means of computational methods. It is found that the enhanced halogen bonding donor ability of these species, in comparison with their demetalated counterparts, translates into a significant acceleration of the Diels-Alder cycloaddition reaction involving cyclohexadiene and methyl vinyl ketone.

The factors behind this acceleration, the *endo-exo* selectivity of the process and the influence of the nature of the transition metal fragment in the activity of these species are quantitatively explored in detail by means of the combination of the Activation Strain Model of reaction and the Energy Decomposition Analysis methods.

Introduction

In the last decade, halogen bonding (XB), defined as the interaction between an electrophilic halogen substituent (called "XB donor") and a nucleophilic Lewis base (called "XB acceptor"), has emerged as a highly useful tool in the fields of supramolecular chemistry, crystal engineering and molecular recognition.^[1,2] In addition, this highly directional interaction has been particularly useful in organocatalysis, increasing the efficiency and in many cases also the selectivity of fundamental transformations in chemistry.^[3] For these reasons, it is not surprising that much effort has been made to increase the strength of the XB by the judicious modification of the XB donors.^[2d] This includes, for instance, electron-deficient aryl iodides or highly fluorinated alkyl iodides,^[4] hydrogen-bond enhanced XB^[5] or even highly electrophilic iodine(III) species.^[6]

In this regard, Kelly and Holman recently reported that the relatively low XB donor ability of iodobenzene and related aryl iodides can be significantly amplified by metalation with the $[\text{CpRu}^{\text{II}}]^+$ fragment, thus forming the corresponding $[\text{CpRu}(\text{ArI})]^+$ metallocene.^[7] The enhanced XB donor ability of these η^6 -metalated aryl iodides is mainly ascribed to a large (ca. 8-fold) increase in the positive potential at the σ -hole of the iodine atom along the C–I bond induced by the transition metal fragment.

Despite the firm structural and spectroscopic evidence supporting the enhancement of the XB donicity in these

metallocenes,^[7] their potential application as organocatalysts remains unexplored so far. Based on our previous studies on the role of the halogen and chalcogen donors as catalysts in fundamental reactions in chemistry,^[8] herein we investigate, by means of state-of-the-art computational methods, the potential catalytic activity of these η^6 -metalated aryl iodides. To this end, the Diels-Alder cycloaddition reaction involving cyclohexadiene and methyl vinyl ketone (MVK) was selected (Scheme 1).

Issues such as the influence of the η^6 -metalated aryl iodides on both the activation barrier and the *endo/exo* selectivity of the process in comparison with the analogous uncatalyzed and demetalated aryl iodide catalyzed cycloaddition reactions as well as the impact of the nature of the transition metal fragment on the transformation shall be quantitatively analyzed in detail with the help of the combination of the Activation Strain Model (ASM)^[9] and Energy Decomposition Method (EDA)^[10] methods. This approach has been selected because it has enormously contributed to our current understanding of fundamental processes in chemistry, and, in particular, of cycloaddition reactions.^[9,11]

Computational Details

Geometry optimizations of the molecules were performed without symmetry constraints using the Gaussian09 (RevD.01) suite of programs^[12] at the dispersion-corrected B3LYP^[13]-D3^[14]/def2-SVP^[15] level including solvent effects (solvent = dichloromethane) with the Polarization Continuum Model (PCM) method.^[16] Reactants and adducts were characterized by frequency calculations and have positive definite Hessian matrices. Transition states show only one

[a] S. Portela, Prof. Dr. I. Fernández

Departamento de Química Orgánica I and Centro de Innovación en Química Avanzada (ORFEO-CINQA)

Facultad de Ciencias Químicas, Universidad Complutense de Madrid
 Ciudad Universitaria, 28040 Madrid (Spain)

E-mail: israel@quim.ucm.es



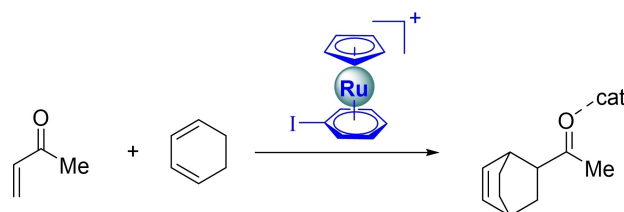
Supporting information for this article is available on the WWW under
<https://doi.org/10.1002/asia.202201214>



This manuscript is part of a joint special collection on Mechanisms and Selectivities of Organic Reactions – In Celebration of Prof. Kendall N. Houk's 80th birthday.



© 2022 The Authors. Chemistry - An Asian Journal published by Wiley-VCH GmbH. This is an open access article under the terms of the Creative Commons Attribution License, which permits use, distribution and reproduction in any medium, provided the original work is properly cited.



Scheme 1. Diels-Alder cycloaddition reaction considered herein.

negative eigenvalue in their diagonalized force constant matrices, and their associated eigenvectors were confirmed to correspond to the motion along the reaction coordinate under consideration using the Intrinsic Reaction Coordinate (IRC) method.^[17] Energy refinements were carried out by means of single-point calculations at the same DFT level using the much larger triple- ζ basis set def2-TZVPP.^[15] This level is denoted PCM(CH₂Cl₂)-B3LYP-D3/def2-TZVPP//PCM(CH₂Cl₂)-B3LYP-D3/def2-SVP. Natural charges were computed using the NBO6.0 method.^[18]

Activation Strain Model (ASM) of Reactivity and Energy Decomposition Analysis (EDA) Methods

Within the ASM method,^[9] also known as the distortion/interaction model,^[9c] the potential energy surface $\Delta E(\zeta)$ is decomposed along the reaction coordinate, ζ , into two contributions, namely the strain $\Delta E_{\text{strain}}(\zeta)$ associated with the deformation (or distortion) required by the individual reactants during the process and the interaction $\Delta E_{\text{int}}(\zeta)$ between these increasingly deformed reactants:

$$\Delta E(\zeta) = \Delta E_{\text{strain}}(\zeta) + \Delta E_{\text{int}}(\zeta)$$

Within the EDA method,^[10] the interaction energy can be further decomposed into the following chemically meaningful terms:

$$\Delta E_{\text{int}}(\zeta) = \Delta V_{\text{elstat}}(\zeta) + \Delta E_{\text{Pauli}}(\zeta) + \Delta E_{\text{orb}}(\zeta) + \Delta E_{\text{disp}}(\zeta)$$

The term ΔV_{elstat} corresponds to the classical electrostatic interaction between the unperturbed charge distributions of the deformed reactants and is usually attractive. The Pauli repulsion ΔE_{Pauli} comprises the destabilizing interactions between occupied orbitals and is responsible for any steric repulsion. The orbital interaction ΔE_{orb} accounts for bond pair formation, charge transfer (interaction between occupied orbitals on one moiety with unoccupied orbitals on the other, including HOMO-LUMO interactions), and polarization (empty-occupied orbital mixing on one fragment due to the presence of another fragment). Finally, the

ΔE_{disp} term accounts for the interactions coming from dispersion forces. Moreover, the NOCV (Natural Orbital for Chemical Valence)^[19] extension of the EDA method has been also used to further partition the ΔE_{orb} term. The EDA-NOCV approach provides pairwise energy contributions for each pair of interacting orbitals to the total bond energy.

The program package ADF^[20] was used for EDA calculations using the optimized PCM(CHCl₃)-B3LYP-D3/def2-SVP geometries at the same B3LYP-D3 level in conjunction with a triple- ζ -quality basis set using uncontracted Slater-type orbitals (STOs) augmented by two sets of polarization functions with a frozen-core approximation for the core electrons.^[21] Auxiliary sets of s, p, d, f, and g STOs were used to fit the molecular densities and to represent the Coulomb and exchange potentials accurately in each SCF cycle.^[22] Scalar relativistic effects were incorporated by applying the zeroth-order regular approximation (ZORA).^[23] This level of theory is denoted ZORA-B3LYP-D3/TZ2P//PCM(CHCl₃)-B3LYP-D3/def2-SVP.

Results and Discussion

The computed reaction profiles for the uncatalyzed (*endo*) Diels-Alder reaction involving MVK and cyclohexadiene and the analogous reactions catalyzed by [CpRu(PhI)]⁺ (**cat1**) and iodobenzene (**cat2**) are shown in Figure 1a. As clearly seen, our calculations indicate that in all cases the cycloaddition proceeds in a concerted yet asynchronous manner through the corresponding six-membered transition state (TS), leading to the exothermic formation of the corresponding cycloadduct. As expected, the catalyzed reactions involve the initial activation of the dienophile, thus forming the halogen bonding complexes **MVK-cat**. From the data in Figure 1a, it becomes evident that the activation of the dienophile is greater for the process mediated by the metallocene catalyst in view of the higher

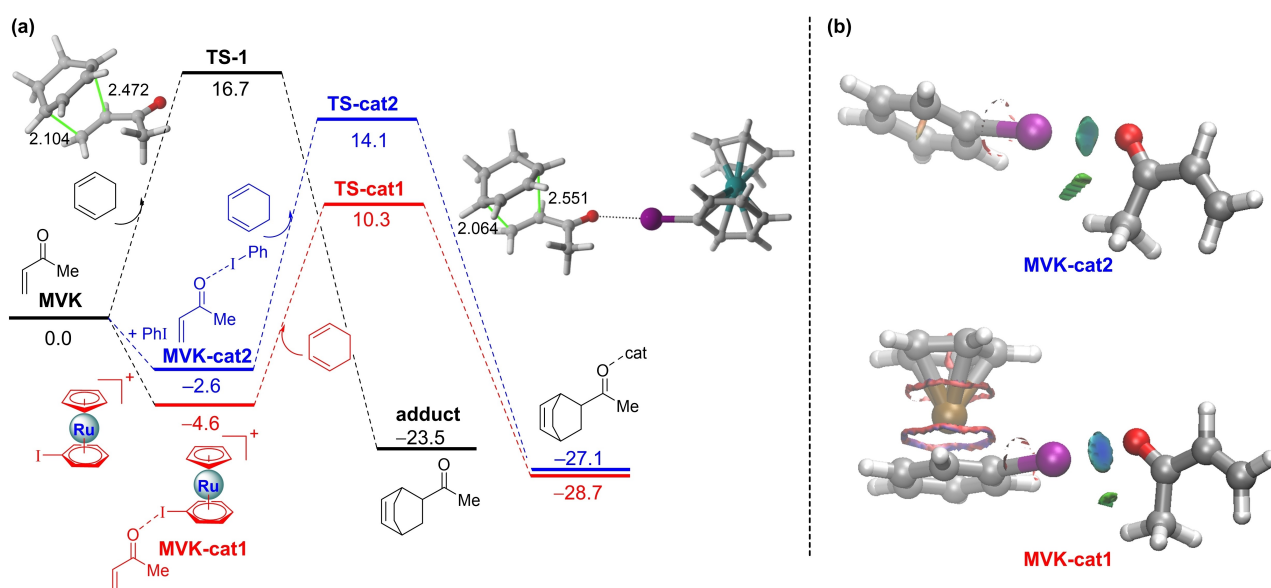


Figure 1. (a) Computed reaction profiles for the parent Diels-Alder cycloaddition reactions between cyclohexadiene and MVK (black), the analogous process catalyzed by **cat1** (red) and **cat2** (blue). Relative energies and bond distances are given in kcal/mol and angstroms, respectively. All data have been computed at the PCM(CH₂Cl₂)-B3LYP-D3/def2-TZVPP//PCM(CH₂Cl₂)-B3LYP-D3/def2-SVP level. (b) Contour plots of the reduced density gradient isosurfaces (density cutoff = 0.045 au) for the **MVK-cat1** and **MVK-cat2** complexes. The greenish surfaces indicate attractive non-covalent interactions.

exothermicity of the formation of **MVK-cat1** in comparison with **MVK-cat2** ($\Delta\Delta E = 2.0$ kcal/mol), which is consistent with the enhanced XB donor ability of **cat1**.^[7] As a consequence, the [CpRu(PhI)]⁺-mediated process becomes much more favored than the analogous uncatalyzed or PhI-catalyzed reactions along the entire reaction coordinate. Indeed, whereas the barrier for the cycloaddition mediated by the low XB donor iodobenzene is nearly identical to that computed for the parent reaction, the **cat1**-mediated reaction proceeds with a lower barrier ($\Delta\Delta E^\ddagger \approx 2$ kcal/mol) in a more exothermic process ($\Delta\Delta E_R \approx -5$ kcal/mol),^[24] which suggests that the η^6 -metallated aryl iodide can indeed be efficiently used as an organocatalyst for this cycloaddition reaction.

Before exploring the factors leading to the acceleration of the cycloaddition induced by the metallocene catalyst, we first investigated the nature of the interaction between the catalyst and the dienophile in the **MVK-cat** complexes. In both cases, according to the NCIPLOT method,^[25] there exists a clear noncovalent attractive interaction (greenish surface) between the iodine atom of the catalyst and the carbonyl oxygen atom of the **MVK** (Figure 1b), which confirms the occurrence of the halogen bonding. Despite that, the computed C=O...I distance is much shorter in the **MVK-cat1** complex (2.742 Å) than in **MVK-cat2** (3.058 Å), which indicates that the halogen bond strength is significantly stronger in the former species as a result of its enhanced XB donor ability.

To further quantitatively understand the enhanced halogen bond in the metallocene complex, the Energy Decomposition Analysis (EDA) method was applied next. As shown in Table 1, the instantaneous interaction energy (ΔE_{int}) between **MVK** and **cat1** is significantly stronger ($\Delta\Delta E_{\text{int}} = 6.3$ kcal/mol) in the **MVK-cat1** complex than that computed for the **MVK-cat2**. This is mainly due to both stronger electrostatic interactions ($\Delta\Delta V_{\text{elstat}} = 8.4$ kcal/mol), and to a lesser extent, also to stronger orbital interactions ($\Delta\Delta E_{\text{orb}} = 3.0$ kcal/mol, dominated by the LP(O) \rightarrow $\sigma^*(\text{I}-\text{C})$ interaction according to the NOCV method). This finding is fully consistent with the significant increase in the positive potential at the σ -hole of the iodine atom reported by Kelly and Holman,^[7] and confirms the predominant electrostatic nature of these and related halogen bonding complexes.^[1,8]

Once the nature of the halogen bonding in the initial activated complexes has been analyzed, we then explored the factors controlling the predicted acceleration for the cycloaddition mediated by the η^6 -metallated phenyl iodide **cat1**. To this end, the Activation Strain Model (ASM) of reactivity was then applied to compare the uncatalyzed and the **cat1**-catalyzed reactions. Figure 2 shows the corresponding activation strain diagrams (ASDs) for both processes from the initial

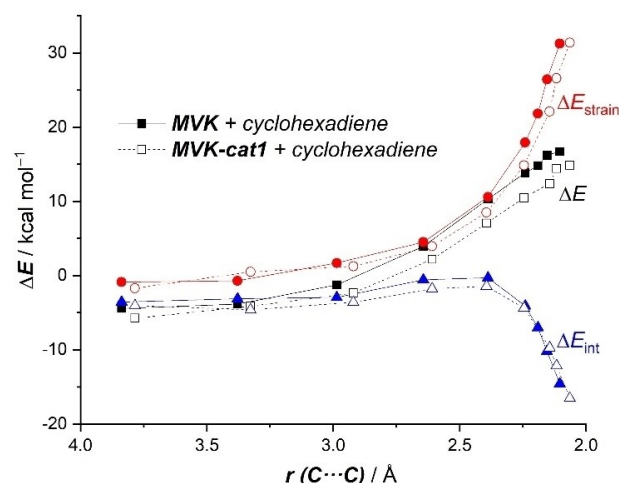


Figure 2. Comparative activation strain analyses of the Diels-Alder cycloadditions reactions between cyclohexadiene and **MVK** (uncatalyzed, solid lines) and **MVK-cat1** (dashed lines) projected onto the shorter C...C bond-forming distance. All data have been computed at the PCM(CH₂Cl₂)-B3LYP-D3/def2-SVP level.

stages of the reaction up to the corresponding transition states and projected onto the shorter C...C bond-forming distance.^[26] Although both transformations exhibit similar ASDs, from the data in Figure 2 it becomes clear that the catalyzed reaction benefits from both a less destabilizing strain energy (measured by the ΔE_{strain} term) and a stronger interaction between the deformed reactants (measured by the ΔE_{int} term) along practically the entire reaction coordinate. Similar to related catalyzed Diels-Alder reactions,^[8c-d,27] the trend in ΔE_{strain} can be ascribed to the extent of the asynchronicity of the cycloaddition, which is markedly higher in the catalyzed reaction according to the higher difference between the newly forming C...C bond lengths in the respective transition states ($\Delta r_{\text{C-C}} = 0.368$ Å vs 0.487 Å for the uncatalyzed and **cat1**-catalyzed reactions, respectively, see also Figure 1a). Thus, a higher asynchronicity implies that the corresponding transition state is reached earlier and consequently, the energy penalty to adopt the transition state geometry (i.e. the activation strain energy) is lower.^[28]

Reasons behind the computed stronger interaction between the deformed reactants for the metallocene-mediated cycloaddition might be initially traced to the stabilization of the π^* -LUMO of the dienophile upon binding to the catalyst, following the traditional LUMO-lowering rationalization in catalysis.^[29] Indeed, our calculations indicate that the LUMO of **MVK-cat1** is stabilized with respect to the parent **MVK** (-2.20 eV vs -1.76 eV, respectively). However, we recently reported that in many instances this LUMO-lowering concept is not the actual factor responsible for the acceleration promoted by different types of catalysts in Diels-Alder reactions but a significant reduction of the Pauli-repulsion between the key occupied π -molecular orbitals of the reactants along the entire coordinate.^[27,30] To check whether this Pauli-repulsion lowering concept is also the key factor behind the computed enhanced interaction for the **cat1**-mediated cycloaddition, the Energy Decomposition Analysis (EDA) method was applied next. As

Table 1. Results of the EDA (energy values in kcal/mol) computed for the **MVK-cat** complexes.^[a]

Compound	ΔE_{int}	ΔE_{Pauli}	ΔV_{elstat}	ΔE_{orb}	ΔE_{disp}
MVK-cat1	−9.6	13.1	−14.4	−6.1	−2.2
MVK-cat2	−3.3	8.0	−6.0	−3.1	−2.1

[a] All data have been computed at the ZORA-B3LYP-D3/TZ2P//PCM(CH₂Cl₂)-B3LYP-D3/def2-SVP level.

depicted in Figure 3, which graphically shows the evolution of the EDA contributors once again for both the uncatalyzed and catalyzed reactions from the initial stages of the reaction up to the corresponding transition states, it becomes clear that the main attractive terms (ΔV_{elstat} and ΔE_{orb}) favor the uncatalyzed reaction. For instance, at the same consistent C...C bond-forming distance of 2.15 Å,^[31] the difference in these terms is $\Delta\Delta V_{\text{elstat}} = 3.8$ kcal/mol and $\Delta\Delta E_{\text{orb}} = 2.1$ kcal/mol, favoring the uncatalyzed reaction, which indicates that neither the electrostatic attractions nor the orbital interactions (despite the more favorable HOMO(diene)-LUMO(dienophile) gap) are responsible for the stronger interaction computed for the metallocene-catalyzed reaction. Instead, this process benefits from a less destabilizing Pauli-repulsion along the entire reaction coordi-

nate ($\Delta\Delta E_{\text{Pauli}} = 2.1$ kcal/mol at 2.15 Å), which confirms that the Pauli-repulsion concept^[30] also applies in this particular catalyzed reaction. This substantial reduction in the Pauli repulsion is mainly due to the polarization induced by the catalyst on the reactive C=C bond of the dienophile away from the incoming diene. This is reflected in a noticeable depopulation of the terminal C=CH₂ carbon atom as confirmed by the computed lower natural charge of this atom in the initial **MVK-cat1** complex ($-0.302e$ vs $-0.321e$ in the parent **MVK**).

Endo-exo selectivity

In agreement with previous reports,^[6,8b] our calculations confirm that the parent cycloaddition reaction between **MVK** and cyclohexadiene is *endo*-selective ($\Delta\Delta E^{\ddagger}_{\text{endo-exo}} = 2.7$ kcal/mol; $\Delta\Delta G^{\ddagger}_{\text{endo-exo}} = 2.6$ kcal/mol). Similarly, the *endo*-approach is also favored in the analogous cycloaddition mediated by the metallocene catalyst **cat1** from both kinetic ($\Delta\Delta E^{\ddagger}_{\text{endo-exo}} = 3.0$ kcal/mol; $\Delta\Delta G^{\ddagger}_{\text{endo-exo}} = 4.0$ kcal/mol) and thermodynamic ($\Delta\Delta E_{\text{endo-exo}} = 1.1$ kcal/mol; $\Delta\Delta G_{\text{endo-exo}} = 1.4$ kcal/mol) points of view.

The reasons behind the *endo*-preference in both processes were then analyzed by means of the ASM approach. Figure 4 shows the corresponding ASDs for both the *endo* and *exo* approaches of both cycloadditions, again from the separate reactants up to the respective transition states. The uncatalyzed and catalyzed transformations exhibit rather similar ASDs in the sense that the interaction energy between the reactants is clearly more stabilizing at the beginning of the process for the *endo*-approach and becomes only slightly stronger at the transition state region. This indicates that the strain energy constitutes the decisive factor leading to the observed *endo*-selectivity, particularly at the proximities of the transition states, where the *endo*-approach benefits from a less destabilizing strain energy (measured by the ΔE_{strain} term). This is similar to

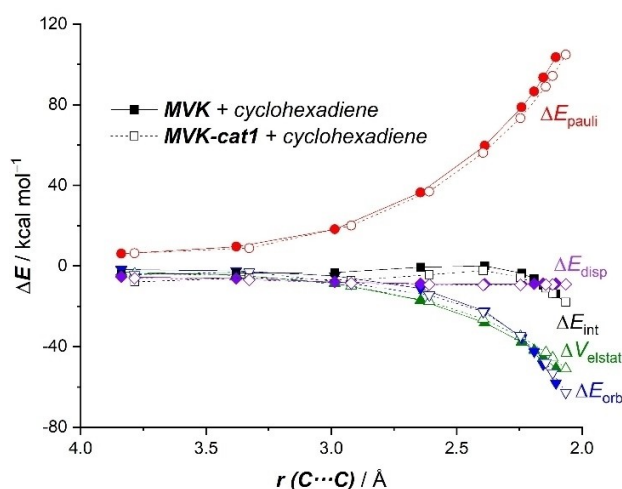


Figure 3. Comparative activation strain analyses of the Diels-Alder cycloaddition reactions between cyclohexadiene and **MVK** (uncatalyzed, solid lines) and **MVK-cat1** (dotted lines) projected onto the shorter C...C bond-forming distance. All data have been computed at the ZORA-B3LYP-D3/TZ2P//PCM(CH₂Cl₂)-B3LYP-D3/def2-SVP level.

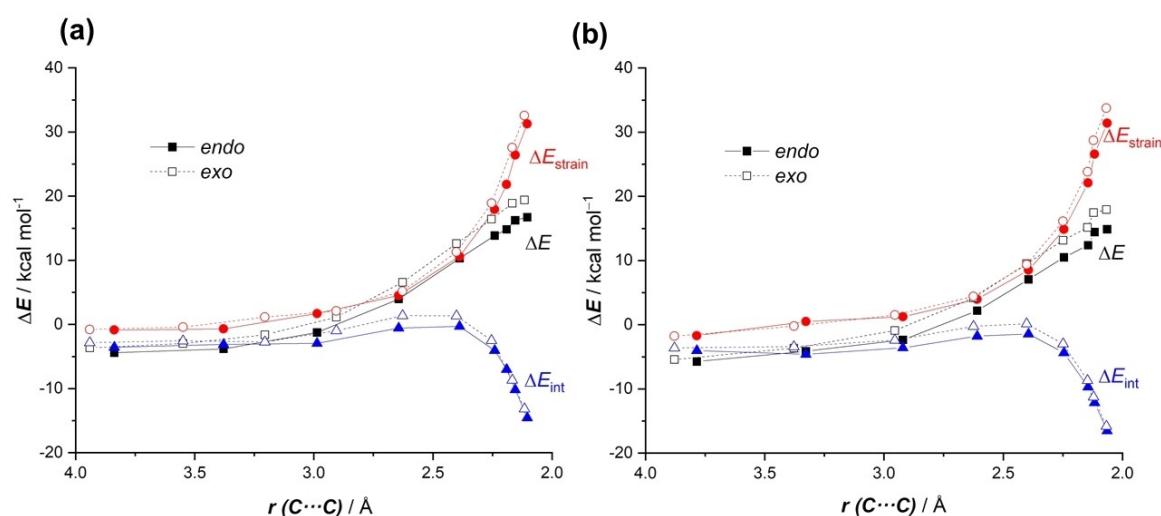


Figure 4. Comparative activation strain analyses for the *endo/exo* approaches of the Diels-Alder cycloadditions reactions between cyclohexadiene and **MVK** (a) and the analogous process mediated by **cat1** (b), projected onto the shorter C...C bond-forming distance. All data have been computed at the PCM(CH₂Cl₂)-B3LYP-D3/def2-TZVPP//PCM(CH₂Cl₂)-B3LYP-D3/def2-SVP level.

the parent cycloaddition reaction between cyclopentadiene and maleic anhydride where the *endo*-selectivity mainly derives exclusively from the distortion energy,^[32] which suggests that the metallocene catalyst has an almost negligible influence on the inherent *endo*-selectivity of the process.

Tuning the activity of the η^6 -metallated aryl iodide catalyst

Aiming at further enhancing the activity (i.e. further reducing the barrier) of the parent η^6 -metallated aryl iodide **cat1**, we finally explored the influence of the transition metal moiety on the same Diels-Alder reaction involving **MVK** and cyclohexadiene (see Figure 5).

The first obvious way to increase the XB donicity of the metallated aryl iodide is by means of the introduction of electron-withdrawing groups (EWGs) in the aryl ring, as done previously for non-metallated systems.^[4] Not surprisingly, the presence of EWGs such as CF_3 , CN or NO_2 groups at the *para* position of the aryl iodide leads to a slight yet noticeable reduction of the activation barrier of the cycloaddition.

We also explored the influence of the transition metal fragment on the process with the PhI ligand unaltered. First, we modified the nature of the transition metal and found that no change in the barrier is observed when using the group 8 $[\text{CpM}^{\text{II}}(\text{PhI})]^+$ analogues ($\text{M}=\text{Fe}, \text{Os}$) as catalysts. At variance, the barrier is significantly reduced for the cycloaddition mediated by the isoelectronic d^6 -neutral $[\text{CpM}^{\text{I}}(\text{PhI})]$ complex^[33] **cat1-Mn** ($\Delta\Delta E=1.5$ kcal/mol with respect to **cat1**), whereas the activity of its heavier group 7 counterparts (**cat1-Tc** and **cat1-Re**) is comparatively lower. A similar reduction in the barrier is found for the isoelectronic- d^6 group 9 $[\text{CpM}^{\text{III}}(\text{PhI})]^{2+}$ complexes **cat1-Co**

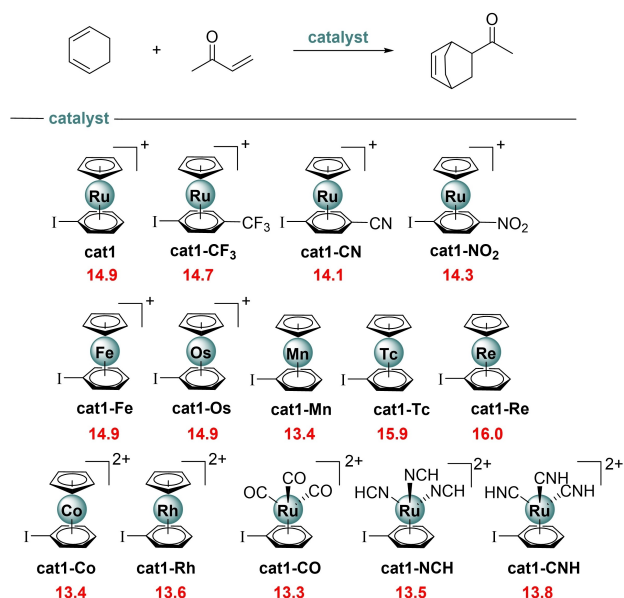


Figure 5. Computed activation barriers (ΔE^\ddagger , in kcal/mol) for the catalyzed cycloaddition reactions involving cyclohexadiene and methyl vinyl ketone. ΔE^\ddagger computed as $\Delta E^\ddagger = E(\text{TS}) - E(\text{cyclohexadiene}) - E(\text{MVK-cat complex})$. All data have been computed at the $\text{PCM}(\text{CH}_2\text{Cl}_2)\text{-B3LYP-D3/def2-TZVP//PCM}(\text{CH}_2\text{Cl}_2)\text{-B3LYP-D3/def2-SVP}$ level.

($\text{M}=\text{Co}$) and **cat1-Rh** ($\text{M}=\text{Rh}$).^[34] Finally, we replaced the cyclopentadienyl ligand with strong π -acceptor ligands to further enhance the electron-withdrawing nature of the transition metal fragment. To our delight, the replacement of the six-electron donor Cp ligand by three two-electron donor CO, nitrile (NCH) or isonitrile (CNH) ligands leads in all cases to a noticeable reduction of the barrier. This initial screening of the nature of the catalyst clearly indicates that the activity of these η^6 -metallated aryl iodides as organocatalysts can be efficiently tuned by rationally modifying the nature of the transition metal fragment.

As mentioned above, the activity of the catalyst is directly related to the activation of the dienophile, which can be estimated by the interaction between **MVK** and the catalyst in the corresponding **MVK-cat** complex. To further support this finding, we applied the EDA method to representative initial complexes of the previous screening (Table 2). As expected, the instantaneous interaction energy (ΔE_{int}) becomes only slightly stronger for the *p*-substituted systems involving **cat1- CF_3** , **cat1-CN** and **cat1- NO_2** which results in a slight decrease in the computed barrier. At variance, rather similar (ΔE_{int}) values were found for the group 8 **MVK-cat1** complexes, which translates into the computed nearly identical barriers for the cycloaddition reactions involving these catalysts. In contrast, the computed interaction is clearly much stronger for the Co(III) species **MVK-cat1-Co** and those complexes having strong acceptor ligands (**MVK-cat1-CO**, **MVK-cat1-NCH** and **MVK-cat1-CNH**), which exhibit the lowest activation barriers. Therefore, our calculations allow us to conclude that the catalytic activity of the metallocene catalyst directly correlates with its XB donor ability.

We finally applied the ASM-EDA approach to understand the origin of the predicted further acceleration in the cycloaddition involving the more active catalysts commented above. To this end, we compared the parent **cat1**-catalyzed reaction ($\Delta E^\ddagger = 14.9$ kcal/mol) with the analogous process mediated by **cat1-NCH** (having 3 nitriles as ligands directly attached to the transition metal, $\Delta E^\ddagger = 13.5$ kcal/mol), as a representative system.

As graphically shown in Figure 6a, the lower barrier computed for the cycloaddition catalyzed by **cat1-NCH** is due to a less destabilizing strain energy along the entire coordinate and, to a lesser extent, to a stronger interaction between the

Table 2. Results of the EDA (energy values in kcal/mol) computed for the **MVK-cat** complexes.^[a]

Compound	ΔE_{int}	ΔE_{Pauli}	ΔV_{elstat}	ΔE_{orb}	ΔE_{disp}
MVK-cat1	−9.6	13.1	−14.4	−6.1	−2.2
MVK-cat1-CF_3	−12.5	14.2	−15.6	−9.0	−2.2
MVK-cat1-CN	−11.2	14.5	−15.9	−7.7	−2.2
MVK-cat1-NO_2	−12.9	14.9	−15.3	−10.2	−2.3
MVK-cat1-Fe	−10.4	13.3	−14.8	−6.8	−2.2
MVK-cat1-Os	−8.2	13.4	−14.6	−4.9	−2.2
MVK-cat1-Co	−24.7	19.8	−24.9	−17.5	−2.2
MVK-cat1-CO	−25.2	22.5	−25.8	−19.5	−2.4
MVK-cat1-NCH	−17.6	17.9	−19.3	−13.6	−2.6
MVK-cat1-CNH	−16.3	18.3	−19.8	−12.2	−2.6

[a] All data have been computed at the $\text{ZORA-B3LYP-D3/TZ2P//PCM}(\text{CH}_2\text{Cl}_2)\text{-B3LYP-D3/def2-SVP}$ level.

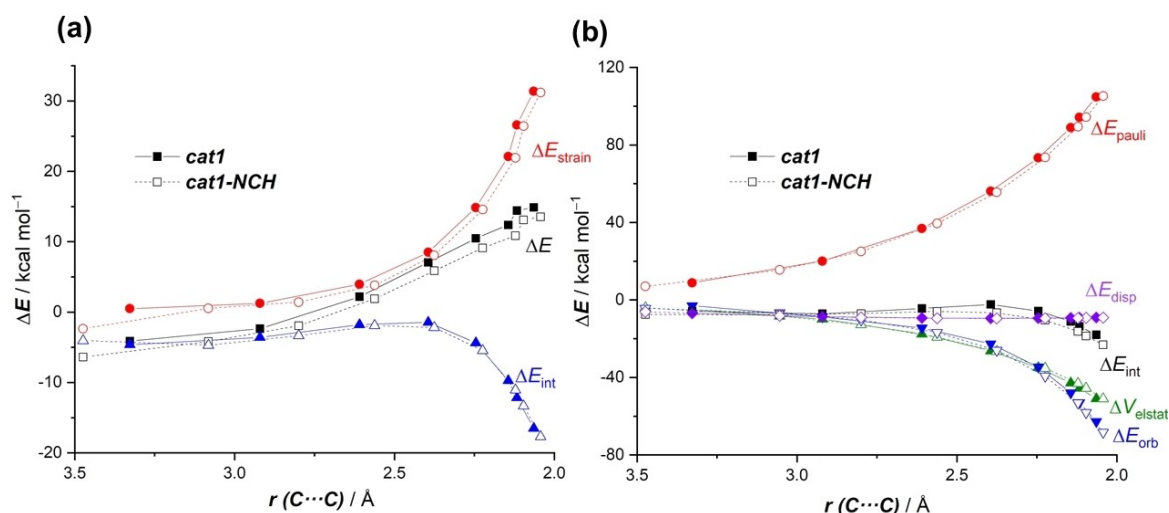


Figure 6. Comparative (a) activation strain analyses (PCM(CH_2Cl_2)-B3LYP-D3/def2-TZVPP//PCM(CH_2Cl_2)-B3LYP-D3/def2-SVP level) and (b) Energy Decomposition Analysis (ZORA-B3LYP-D3/TZ2P//PCM(CH_2Cl_2)-B3LYP-D3/def2-SVP level) of the Diels-Alder cycloadditions reactions between cyclohexadiene and **MVK-*cat1*** (solid lines) and **MVK-*cat1-NCH*** (dashes lines) projected onto the shorter C...C bond-forming distance.

deformed reactants. Once again, the less destabilizing ΔE_{strain} is ascribed to a further increase in the asynchronicity of the reaction as confirmed by the computed C...C bond-forming distances in the corresponding transition state: 2.043 and 2.606 Å, which is translated into $\Delta r_{\text{C-C}} = 0.563 \text{ \AA}$ ($> \Delta r_{\text{C-C}} = 0.487 \text{ \AA}$ for the process mediated by *cat1*). The slightly stronger interaction computed for this cycloaddition is due, according to the EDA method (Figure 6b), once again mainly to a reduction of the Pauli repulsion between the key π -molecular orbitals of both reactants and also, albeit to a much lesser extent, to stronger orbital interactions at the transition state region. Not surprisingly, the further reduction of the Pauli repulsion is again directly related to a higher depopulation of the reactive C=C of the dienophile, which is confirmed by an even lower natural charge at the terminal C=CH₂ carbon atom in the corresponding **MVK-*cat1-NCH*** complex (−0.293e vs −0.302e in **MVK-*cat1***).

Conclusion

From the computational study reported herein, it is predicted that η^6 -metalated aryl iodides can be used as organocatalysts for the Diels-Alder cycloaddition reaction involving cyclohexadiene and methyl vinyl ketone. These species induce a noticeable acceleration of the process by reducing the corresponding activation barrier up to 3–4 kcal/mol with respect to the parent uncatalyzed reaction or the analogous process involving the corresponding demetalated aryl iodide without modifying the innate *endo*-selectivity of the transformation. The metallocene catalyst binds the carbonyl group of the dienophile through a halogen bond, whose strength can be efficiently modulated by increasing the acceptor nature of the transition metal fragment. This non-covalent interaction induces a significant depopulation of the key $\pi\text{-C}=\text{C}$ molecular orbital of the dienophile which translates into a reduction of the Pauli repulsion between the reactants along the entire reaction

coordinate. As a result, the interaction energy between the reactants becomes stronger than that in the parent uncatalyzed reaction. In addition, the catalyst also increases the asynchronicity of the reaction which leads to a less destabilizing strain energy. Therefore, the catalytic activity of these η^6 -metalated aryl iodides, which can be efficiently tuned, finds its origin in both a higher asynchronicity of the process and a reduction of the Pauli repulsion between the deformed reactants.

Acknowledgements

This work was supported by the Spanish MCIN/AEI/10.13039/501100011033 (Grants PID2019-106184GB-I00 and RED2018-102387-T). S. P. acknowledges the MCIN for a FPI grant.

Conflict of Interest

The authors declare no conflict of interest.

Data Availability Statement

The data that support the findings of this study are available in the supplementary material of this article.

Keywords: DFT calculations · Diels-Alder · halogen bonding · metallocenes · reactivity

- [1] a) P. Metrangolo, G. Resnati, in *Halogen Bonding I*, Springer, Berlin, 2015; b) P. Metrangolo, G. Resnati, in *Halogen Bonding II*, Springer, Berlin, 2015.
- [2] a) M. Erdélyi, *Chem. Soc. Rev.* **2012**, 41, 3547–3557; b) A. Mukherjee, S. Tothadi, G. R. Desiraju, *Acc. Chem. Res.* **2014**, 47, 2514–2524; c) P. Metrangolo, H. Neukirch, T. Pilati, G. Resnati, *Acc. Chem. Res.* **2005**, 38,

- 386–395; d) G. Cavallo, P. Metrangolo, R. Milani, T. Pilati, A. Priimagi, G. Resnati, G. Terraneo, *Chem. Rev.* **2016**, *116*, 2478–2601.
- [3] For representative recent reviews, see: a) D. Bulfield, S. M. Huber, *Chem. Eur. J.* **2016**, *22*, 14434–14450; b) R. L. Sutar, S. M. Huber, *ACS Catal.* **2019**, *9*, 9622–9639; c) M. Breugst, J. J. Koenig, *Eur. J. Org. Chem.* **2020**, 5473–5487.
- [4] a) R. J. Mayer, A. R. Ofial, H. Mayr, C. Y. Legault, *J. Am. Chem. Soc.* **2020**, *142*, 5221–5233; b) D. L. Reinhard, F. Heinen, J. Stoesser, E. Engelage, S. M. Huber, *Helv. Chim. Acta* **2021**, *104*, No. e2000221.
- [5] a) D. A. Decato, A. M. S. Riel, J. H. May, V. S. Bryantsev, O. B. Berryman, *Angew. Chem. Int. Ed.* **2021**, *60*, 3685–3692; *Angew. Chem.* **2021**, *133*, 3729–3736; b) A. M. S. Riel, D. A. Decato, J. Suna, O. B. Berryman, *Chem. Commun.* **2022**, 58, 1378–1381.
- [6] F. Heinen, D. L. Reinhard, E. Engelage, S. M. Huber, *Angew. Chem. Int. Ed.* **2021**, *60*, 5069–5073; *Angew. Chem.* **2021**, *133*, 5127–5132.
- [7] A. W. Kelly, K. T. Holman, *Angew. Chem. Int. Ed.* **2022**, *61*, e202115556.
- [8] a) T. Hamlin, I. Fernández, F. M. Bickelhaupt, *Angew. Chem. Int. Ed.* **2019**, *58*, 8922–8926; *Angew. Chem.* **2019**, *131*, 9015–9020; b) S. Portela, J. J. Cabrera-Trujillo, I. Fernández, *J. Org. Chem.* **2021**, *86*, 5317–5326; c) S. Portela, I. Fernández, *Eur. J. Org. Chem.* **2021**, 6102; d) S. Portela, I. Fernández, *Tetrahedron Chem.* **2022**, *1*, 100008.
- [9] a) I. Fernández, F. M. Bickelhaupt, *Chem. Soc. Rev.* **2014**, *43*, 4953–4967; b) L. P. Wolters, F. M. Bickelhaupt, *WIREs Comput. Mol. Sci.* **2015**, *5*, 324–343; c) F. M. Bickelhaupt, K. N. Houk, *Angew. Chem. Int. Ed.* **2017**, *56*, 10070–10086; *Angew. Chem.* **2017**, *129*, 10204–10221. See also; d) I. Fernández, in *Discovering the Future of Molecular Sciences* (Ed.: B. Pignataro), Wiley-VCH, Weinheim, **2014**, pp. 165–187.
- [10] For reviews on the EDA method, see: a) F. M. Bickelhaupt, E. J. Baerends, in *Reviews in Computational Chemistry*, (Eds. K. B. Lipkowitz, D. B. Boyd), Wiley-VCH: New York, **2000**, Vol. 15, pp. 1–86; b) M. von Hopffgarten, G. Frenking, *WIREs Comput. Mol. Sci.* **2012**, *2*, 43–62; c) I. Fernández, in *Applied Theoretical Organic Chemistry*, (Ed. D. J. Tantillo), World Scientific, New Jersey, **2018**, pp. 191–226.
- [11] Selected recent representative examples: a) D. N. Kamber, S. S. Nguyen, F. Liu, J. S. Briggs, H.-W. Shih, R. D. Row, Z. G. Long, K. N. Houk, Y. Liang, J. A. Prescher, *Chem. Sci.* **2019**, *10*, 9109–9114; b) A. Couce-Ríos, A. Lledós, I. Fernández, G. Ujaque, *ACS Catal.* **2019**, *9*, 848–858; c) Gallardo-Fuentes, R. Ormazábal-Toledo, I. Fernández, *J. Org. Chem.* **2020**, *85*, 9272–9280; d) I. Fernández, *Chem. Sci.* **2020**, *11*, 3769–3779; e) T. Hansen, P. Vermeeren, F. M. Bickelhaupt, T. A. Hamlin, *Angew. Chem. Int. Ed.* **2021**, *60*, 20840–20848; *Angew. Chem.* **2021**, *133*, 21008–21016; f) I. Fernández, *Chem. Commun.* **2022**, 58, 4931–4940.
- [12] Gaussian 09, Revision D.01, M. J. Frisch, G. W. Trucks, H. B. Schlegel, G. E. Scuseria, M. A. Robb, J. R. Cheeseman, G. Scalmani, V. Barone, G. A. Petersson, H. Nakatsuji, X. Li, M. Caricato, A. Marenich, J. Bloino, B. G. Janesko, R. Gomperts, B. Mennucci, H. P. Hratchian, J. V. Ortiz, A. F. Izmaylov, J. L. Sonnenberg, D. Williams-Young, F. Ding, F. Lipparini, F. Egidi, J. Goings, B. Peng, A. Petrone, T. Henderson, D. Ranasinghe, V. G. Zakrzewski, J. Gao, N. Rega, G. Zheng, W. Liang, M. Hada, M. Ehara, K. Toyota, R. Fukuda, J. Hasegawa, M. Ishida, T. Nakajima, Y. Honda, O. Kitao, H. Nakai, T. Vreven, K. Throssell, J. A. Montgomery, Jr., J. E. Peralta, F. Ogliaro, M. Bearpark, J. J. Heyd, E. Brothers, K. N. Kudin, V. N. Staroverov, T. Keith, R. Kobayashi, J. Normand, K. Raghavachari, A. Rendell, J. C. Burant, S. S. Iyengar, J. Tomasi, M. Cossi, J. M. Millam, M. Klene, C. Adamo, R. Cammi, J. W. Ochterski, R. L. Martin, K. Morokuma, O. Farkas, J. B. Foresman, D. J. Fox, Gaussian, Inc., Wallingford CT, **2016**.
- [13] a) A. D. Becke, *J. Chem. Phys.* **1993**, *98*, 5648–5652; b) C. Lee, W. Yang, R. G. Parr, *Phys. Rev. B* **1998**, *37*, 785–789; c) S. H. Vosko, L. Wilk, M. Nusair, *Can. J. Phys.* **1980**, *58*, 1200–1211.
- [14] S. Grimme, J. Antony, S. Ehrlich, H. Krieg, *J. Chem. Phys.* **2010**, *132*, 154104–19.
- [15] F. Weigend, R. Ahlrichs, *Phys. Chem. Chem. Phys.* **2005**, *7*, 3297–3305.
- [16] a) S. Miertuš, E. Scrocco, J. Tomasi, *Chem. Phys.* **1981**, *55*, 117–129; b) J. L. Pascual-Ahuir, E. Silla, I. Tuñón, *J. Comput. Chem.* **1994**, *15*, 1127–1138; c) V. Barone, M. Cossi, *J. Phys. Chem. A* **1998**, *102*, 1995–2001.
- [17] C. Gonzalez, H. B. Schlegel, *J. Phys. Chem.* **1990**, *94*, 5523–5527.
- [18] E. D. Glendenning, C. R. Landis, F. Weinhold, *J. Comput. Chem.* **2013**, *34*, 1429–1437.
- [19] M. P. Mitoraj, A. Michalak, T. Ziegler, *J. Chem. Theory Comput.* **2009**, *5*, 962–975.
- [20] a) G. Te Velde, F. M. Bickelhaupt, E. J. Baerends, C. Fonseca Guerra, S. J. A. Van Gisbergen, J. G. Snijders, T. Ziegler, *J. Comput. Chem.* **2001**, *22*, 931–967; b) *ADF2020*, SCM, Theoretical Chemistry, Vrije Universiteit, Amsterdam, The Netherlands, <http://www.scm.com>.
- [21] J. G. Snijders, P. Vernooijs, E. J. Baerends, *At. Data Nucl. Data Tables* **1981**, *26*, 483–574.
- [22] J. Krijn, E. J. Baerends, *Fit Functions in the HFS-Method*, Internal Report (in Dutch), Vrije Universiteit Amsterdam, The Netherlands, **1984**.
- [23] a) E. van Lenthe, E. J. Baerends, J. G. Snijders, *J. Chem. Phys.* **1993**, *99*, 4597–4610; b) E. van Lenthe, E. J. Baerends, J. G. Snijders, *J. Chem. Phys.* **1994**, *101*, 9783–9792; c) E. van Lenthe, A. Ehlers, E. J. Baerends, *J. Chem. Phys.* **1999**, *110*, 8943–8953.
- [24] To check the reliability of the selected method, we also used the computed at the more accurate M06-2X/def2-SVP level. Rather similar barrier energy difference ($\Delta\Delta E^\ddagger = 1.4$ kcal/mol) was computed, thus providing further support to the selected DFT method.
- [25] E. R. Johnson, S. Keinan, P. Mori-Sánchez, J. Contreras-García, A. J. Cohen, W. Yang, *J. Am. Chem. Soc.* **2010**, *132*, 6498–6506.
- [26] This critical reaction coordinate undergoes a well-defined change throughout the reaction and has successfully been used in the past for the analysis of other [4+2]-cycloaddition reactions. See, for instance, a) I. Fernández, *Phys. Chem. Chem. Phys.* **2014**, *16*, 7662–7671; b) I. Fernández, *Eur. J. Org. Chem.* **2018**, 1394–1402. See also Ref. [8b–d] and [11d].
- [27] a) P. Vermeeren, T. A. Hamlin, I. Fernández, F. M. Bickelhaupt, *Angew. Chem. Int. Ed.* **2020**, *59*, 6201–6206; *Angew. Chem.* **2020**, *132*, 6260–6265; b) P. Vermeeren, T. A. Hamlin, I. Fernández, F. M. Bickelhaupt, *Chem. Sci.* **2020**, *11*, 8105–8112.
- [28] For a recent study on the factors leading to the asynchronicity of Diels-Alder reactions, see: P. Vermeeren, T. A. Hamlin, F. M. Bickelhaupt, *Phys. Chem. Chem. Phys.* **2021**, *23*, 20095–20106.
- [29] J. Clayden, S. Greeves, S. Warren, in *Organic Chemistry*, Oxford University Press, second ed.
- [30] T. A. Hamlin, F. M. Bickelhaupt, I. Fernández, *Acc. Chem. Res.* **2021**, *54*, 1972–1981.
- [31] Performing this analysis at a consistent point along the reaction coordinate (near all transition structures), rather than the transition state alone, ensures that the results are not skewed by the position of the transition state.
- [32] I. Fernández, F. M. Bickelhaupt, *J. Comput. Chem.* **2014**, *35*, 371–376.
- [33] H. Braunschweig, A. Damme, K. Dück, M. Fuß, C. Hörl, T. Kramer, I. Krummenacher, T. Kupfer, V. Paprocki, C. Schneider, *Chem. Eur. J.* **2015**, *21*, 14797–14803.
- [34] a) C. White, P. M. Maitlis, *J. Chem. Soc. A* **1971**, 3322–3326; b) D. A. Loginov, M. M. Vinogradov, Z. A. Starikova, P. V. Petrovskii, A. R. Kudinov, *Russ. Chem. Bull.* **2004**, *53*, 1949–1953.

Manuscript received: December 1, 2022
Revised manuscript received: December 12, 2022
Accepted manuscript online: December 14, 2022
Version of record online: December 29, 2022